ChemPubSoc Europe

DOI: 10.1002/chem.201404377

CHEMISTRY
A European Journal
Full Paper

Metal–Organic Frameworks

Mixed-Metal MIL-100(Sc,M) (M = Al, Cr, Fe) for Lewis Acid Catalysis and Tandem C–C Bond Formation and Alcohol Oxidation

Laura Mitchell,[a] Patrick Williamson,[a] Barbora Ehrlichová,[a] Amanda E. Anderson,[a] Valerie R. Seymour,[a] Sharon E. Ashbrook,[a] Nadia Acerbi,[b] Luke M. Daniels,[c] Richard I. Walton,[c] Matthew L. Clarke,*[a] and Paul A. Wright*[a]

Abstract: The trivalent metal cations Al^{3+}, Cr^{3+}, and Fe^{3+} were each introduced, together with Sc^{3+}, into MIL-100(Sc,M) solid solutions (M = Al, Cr, Fe) by direct synthesis. The substitution has been confirmed by powder X-ray diffraction (PXRD) and solid-state NMR, UV/Vis, and X-ray absorption (XAS) spectroscopy. Mixed Sc/Fe MIL-100 samples were prepared in which part of the Fe is present as α-Fe_2O_3 nanoparticles within the mesoporous cages of the MOF, as shown by XAS, TGA, and PXRD. The catalytic activity of the mixed-metal catalysts in Lewis acid catalysed Friedel–Crafts additions increases with the amount of Sc present, with the attenuating effect of the second metal decreasing in the order Al > Fe > Cr. Mixed-metal Sc,Fe materials give acceptable activity: 40% Fe incorporation only results in a 20% decrease in activity over the same reaction time and pure product can still be obtained and filtered off after extended reaction times. Supported α-Fe_2O_3 nanoparticles were also active Lewis acid species, although less active than Sc^{3+} in trimer sites. The incorporation of Fe^{3+} into MIL-100(Sc) imparts activity for oxidation catalysis and tandem catalytic processes (Lewis acid + oxidation) that make use of both catalytically active framework Sc^{3+} and Fe^{3+}. A procedure for using these mixed-metal heterogeneous catalysts has been developed for making ketones from (hetero)aromatics and a hemiacetal.

Introduction

The current intense interest in metal–organic frameworks (MOFs) derives from the great structural and chemical variety they offer and the wide range of novel properties they exhibit, including very high permanent porosity in some cases, with associated potential applications. Interest has concentrated mainly on their adsorption and separation properties and particularly their high capacities and selectivities in the adsorption of fuel-related gases,[1–3] but the last few years have seen increasing focus on the use of porous metal–organic frameworks in catalysis.[4–8] Part of the attraction of MOFs as catalysts is the opportunity they offer to prepare, optimise, and apply crystallographically well-defined single site heterogeneous catalysts of the type defined by Thomas.[9,10] The summary by Furukawa et al. of many of the most interesting reports of their catalytic performance, which includes reference to their use in more than 50 different reactions, illustrates their potential and their versatility,[11] while Dhakshinamoorthy and Garcia have critically reviewed the activity of MOFs specifically in oxidation catalysis.[7] The field of MOF catalysis is far from mature, however, with the current literature dominated by proof-of-concept studies of catalytic activity of MOF frameworks in model reactions, and also investigations in which the MOF acts as a scaffold to support metal nanoparticles[8,12–16] or catalytically active organometallic or coordination complexes bound to the organic struts linking the metal centres.[17–20] The most advanced of the latter have investigated chiral MOFs as supports and ligands for enantioselective catalysis.[21–23]

For those catalytic reactions where it is the metal cations integral to the MOF framework that are the catalytically active sites, the use of MOFs in Lewis acid-catalysed reactions has been particularly well-explored, especially for materials where coordinatively unsaturated sites can be generated throughout the pore space. Copper-bearing HKUST-1[14,24–26] and iron- and chromium-bearing MIL-100 and MIL-101,[27–31] for example, have been investigated extensively as Lewis acids, and much recent progress has been made in optimizing the zirconium terephthalate-based MOF, UiO-66 as a Lewis acid catalyst by defect manipulation and ligand functionalisation.[32,33] We recently introduced the scandium trimesate MIL-100(Sc)[34] into this arena of Lewis acid catalysis.[35] The MIL-100 framework[36]

[a] L. Mitchell, P. Williamson, B. Ehrlichová, A. E. Anderson, V. R. Seymour, S. E. Ashbrook, M. L. Clarke, P. A. Wright
EaStCHEM School of Chemistry, University of St Andrews
Purdie Building, North Haugh, St. Andrews, Fife, KY16 9ST (UK)
Fax: (+44) 1334-463808
E-mail: mc28@st-andrews.ac.uk
paw2@st-andrews.ac.uk

[b] N. Acerbi
Johnson Matthey Technology Centre
Blount's Court Road, Sonning Common, Reading, RG4 9NH (UK)

[c] L. M. Daniels, R. I. Walton
Department of Chemistry, University of Warwick
Coventry, CV4 7AL (UK)

Supporting information for this article is available on the WWW under http://dx.doi.org/10.1002/chem.201404377.

is made up of trimesate (benzene tricarboxylate, BTC) groups linked by trivalent metal (M) trimers, framework formula $M_3OX_3(BTC)_2$, where X represents coordinating ligands on M^{3+} cations, one of which must carry a single negative charge to maintain neutrality where all three metal cations are trivalent. It contains a three dimensionally connected pore space that comprises two different types of mesoporous cage (Figure 1).

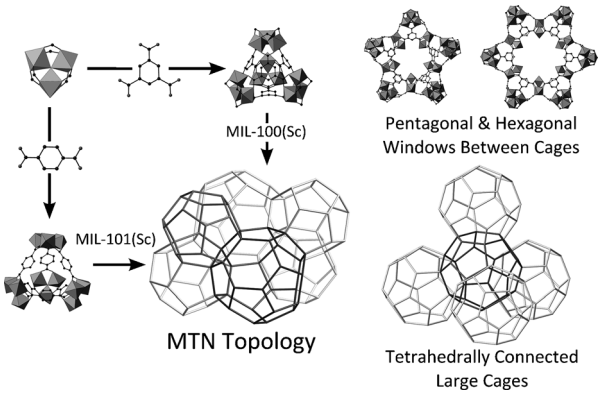

Figure 1. Structure of MIL-100, showing the assembly of trimer $Sc_3O(O_2C\text{-})_6$ units via supertetrahedra to give networks containing two kinds of cage. Reproduced from Ref. [34] with permission.

This material was compared with a wide range of microporous and mesoporous MOFs that can have coordinatively unsaturated metal sites for Lewis acid-catalysed reactions such as the carbonyl ene reaction of ethyl glyoxylate derivatives (including tandem deprotection–ene reactions), Friedel–Crafts-type Michael additions, and imine formation. In each case it outperformed other much-cited MOFs and was shown to be a fully heterogeneous catalyst that could be re-used without significant loss of activity, crystallinity, or porosity.

We report herein the synthesis and full characterisation of mixed-metal MIL-100(Sc,M^{3+}), where M is cheap and readily available Al^{3+} or Fe^{3+} that replaces Sc^{3+} in the scandium trimers ($Sc_3OX_3(O_2C\text{—})_6$), which are the metal-based nodes that are the building units of MIL-100(Sc). The aims were to make the use of this catalyst more economic without strongly decreasing its activity, and more importantly for MIL-100(Sc,Fe), to investigate the use of mixed-metal MOFs to perform catalytic reactions in which each of the catalytic active metals plays a different role. MIL-100(Fe) has previously been reported for its activity in oxidation catalysis[29–31,37] and iron is also an environmentally acceptable and non-toxic metal. For further comparison of the effect of metal substitution on the activity of MIL-100(Sc) as a Lewis acid catalyst, a series of MIL-100(Sc,Cr) materials was also prepared.

In our approach to preparing mixed-metal MOFs that are catalytically bifunctional, both Sc^{3+} and Fe^{3+} are present as cations within framework sites. The prospect of including two or more catalytic functionalities in the same materials is attractive, as it offers the potential to perform sequential reactions with reduced diffusion paths for intermediates, as recently emphasized by a review of cascade reactions catalysed by MOFs.[38] Other approaches to preparing MOFs containing two metals with different catalytic functionalities include nanoparticles supported onto Lewis acidic MOFs and catalytically active materials made from ligands that are further coordinated to "extra-framework" metal cations. However, we are not aware of any precedents where two framework metals contribute in a complementary way towards a catalytic process. Herein we show that a mixed-metal MIL-100(Sc,Fe) catalyst can enable a tandem deacetalisation–Friedel–Crafts addition followed by alcohol oxidation. The Sc^{3+} Lewis acid sites are the more active in the first two stages of the reaction, with the Fe^{3+} sites being responsible for the oxidation catalysis.

Along with preparing and testing MIL-100(Sc,Fe) with all trivalent cations in trimer sites, we present a route to the direct synthesis of MIL-100(Sc,Fe)XS materials that also contain nanoparticles of α-Fe_2O_3 in their pores. These show enhanced specific activity in Lewis acid catalysis compared with MIL-100(Sc,Fe) materials at the same Fe content, but are not as active in bifunctional catalysis.

Results and Discussion

Synthesis and characterisation

Mixed-metal MIL-100(Sc,M) samples were prepared using our published route[34,35] to the synthesis of MIL-100(Sc) and substituting a portion of the Sc^{III} source (aqueous $ScCl_3$ solution) by $Al(NO_3)_3{\cdot}9H_2O$, $CrCl_3{\cdot}6H_2O$, or $FeCl_3{\cdot}6H_2O$. A second series of MIL-100 samples containing scandium and iron was prepared in which an excess of the trivalent metal salts over the trimesic acid was added during synthesis. MIL-100(Sc) is normally synthesised using three equivalents of a scandium salt to two equivalents of ligand. It was found that when using a ratio of three equivalents of Sc^{III} salt and one equivalent of Fe^{III} salt with two equivalents of ligand there was no evidence of iron becoming incorporated in the MIL-100(Sc), and so it was inferred that scandium is incorporated preferentially. Reducing the amount of Sc^{III} salt to two equivalents and adding two to five equivalents of Fe^{III} salt (also with two equivalents of ligand) gave a range of samples with distinct colour and spectroscopic properties, later found to contain α-Fe_2O_3, and these are described below as the MIL-100(Sc,Fe)XS series (see Table 1 for details).

PXRD patterns of the MIL-100(Sc,Fe), MIL-100(Sc,Al), and MIL-100(Sc,Cr) series of materials are given in the Supporting Information, Figures S 1.1–3. All indicate that MIL-100 is the only crystalline phase present. Unit cell determination was performed by structureless Le Bail refinement within the GSAS suite of programs[39,40] against laboratory PXRD (Supporting Information). The elemental metal compositions of the samples (Sc, Al, Cr, Fe) were measured by selected-area energy-dispersive X-ray (EDX) analysis and found to be uniform over particles of the solid. The measured Sc:M atomic ratios in the crystals are similar to those of the syntheses of the MIL-100 samples (Table 1). The porosity of these materials was measured by N_2 adsorption on methanol-washed materials heated at 423 K

Table 1. Details of syntheses and characterization[a] of MIL-100(Sc,M) samples.

Sample name	Synthesis molar ratio M_1:M_2:BTC:DMF	EDX Sc:M molar ratio	Cubic axis *a* [Å]	TGA residue [wt%]	Pore volume[b] [$cm^3\ g^{-1}$]
MIL-100(Sc)	3:0:2:600	–	75.4360(8)	26.2	0.61
MIL-100($Sc_{80}Al_{20}$)	2.4:0.6:2:600	78.9:21.1	74.9231(21)	26.4	0.56
MIL-100($Sc_{60}Al_{40}$)	1.8:1.2:2:600	63.2:36.8	74.6841(12)	25.2	0.57
MIL-100($Sc_{40}Al_{60}$)	1.2:1.8:2:600	42.0:58.0	74.3204(7)	24.5	0.55
MIL-100($Sc_{20}Al_{80}$)	0.6:2.4:2:600	19.4:80.6	73.9127(16)	22.9	0.54
MIL-100(Al)	3:0:2:600	–	73.2356(2)	22.2	0.54
MIL-100($Sc_{80}Cr_{20}$)	2.4:0.6:2:600	80.2:19.8	75.1452(2)	27.1	0.59
MIL-100($Sc_{60}Cr_{40}$)	1.8:1.2:2:600	62.5:37.5	74.8045(12)	28.5	0.58
MIL-100($Sc_{40}Cr_{60}$)	1.2:1.8:2:600	35.1:64.9	74.6121(15)	28.9	0.59
MIL-100($Sc_{20}Cr_{80}$)	0.6:2.4:2:600	12.9:87.1	74.3145(5)	30.2	0.54
MIL-100(Cr)		–	73.6525(19)	30.5	0.60
MIL-100($Sc_{80}Fe_{20}$)	2.4:0.6:2:600	80.2/19.8	75.0561(14)	27.4	0.58
MIL-100($Sc_{60}Fe_{40}$)	1.8:1.2:2:600	58.3:47.7	74.553(31)	28.9	0.60
MIL-100($Sc_{40}Fe_{60}$)	1.2:1.8:2:600	36.3:63.7	74.5501(14)	29.5	0.59
MIL-100($Sc_{20}Fe_{80}$)	0.6:2.4:2:600	21.4/78.6	74.22093(16)	31.7	0.59
MIL-100(Fe)		–	73.5821(4)	32.4	0.59
MIL-100($Sc_{80}Fe_{20}$)XS[c]	2:3:2:600	78.2:21.8	75.2241(6)	36.2	0.56
MIL-100($Sc_{60}Fe_{40}$)XS	2:4:2:600	63.8:36.2	75.0666(18)	38.4	0.45
MIL-100($Sc_{50}Fe_{50}$)XS	2:5:2:600	48.8:51.2	74.9223(14)	48.1	0.38

[a] After washing with methanol and removal by drying. [b] Measured by N_2 adsorption at 77 K, at $p/p_0 = 0.9$. [c] XS refers to samples prepared with metal cation amount in synthesis gel in excess of that required stoichiometrically for MIL-100. Subscripts after Sc and M refer to mole percent of metal cations present.

under a dynamic vacuum of 10^{-5} mbar for 16 h prior to examination, and the details are given in Table 1.

For the MIL-100(Sc,Cr) series, the substitution of Cr^{3+} for Sc^{3+} is confirmed by the increase in UV absorbance (Supporting Information, Figure S3.1) and the decrease in unit cell parameter (Figure 2), which occurs because Cr^{3+} (0.615 Å) is smaller than Sc^{3+} (0.745 Å).[41]

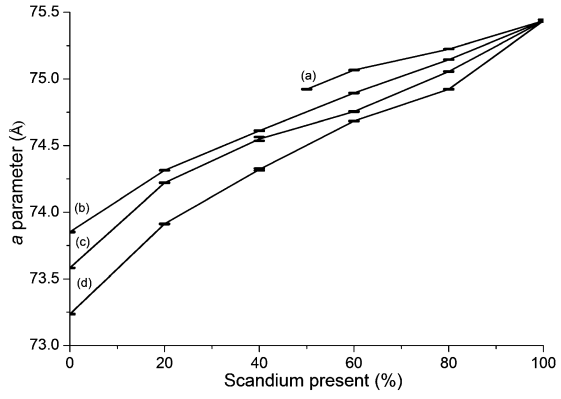

Figure 2. The cubic unit cell *a* parameter of a) MIL-100(Sc,Fe)XS, b) MIL-100(Sc,Cr), c) MIL-100(Sc,Fe), and d) MIL-100(Sc,Al) series.

For the MIL-100(Sc,Al) series, evidence that the Al^{3+} is incorporated in octahedral sites within the scandium-based trimers was obtained by unit cell determination and by solid-state NMR spectroscopy. The cubic unit cell parameter of the samples shows a uniform decrease from 75.436(8) Å for MIL-100(Sc) to 72.958(2) Å for the $Sc_{20}Al_{80}$ material (Figure 2). This is expected owing to the smaller size of octahedral Al^{3+} (ionic radius 0.535 Å) compared to octahedral Sc^{3+} (0.745 Å).[41]

The solid-state ^{27}Al MAS NMR spectra (Figure 3) display a single asymmetric resonance ($\delta = -2.5$ ppm) consistent with the presence of AlO_6 octahedra in the $M_3OX_3(O_2C{-})_6$ trimer units of MIL-100,[42] but they give no unambiguous evidence for the presence or absence of mixed Al/Sc trimers. The ^{45}Sc MAS NMR spectra (Figure 3) also show an asymmetric lineshape, again suggesting the presence of disorder (and a distribution of NMR parameters), while the resonance position appears characteristic of octahedral Sc in trimer units.[34] The ^{45}Sc MAS lineshapes, however, do appear to contain two distinct components. The broader component, centred at lower δ, can be attributed to a Sc atom with a terminal OH group attached (exhibiting larger quadrupolar coupling values, C_Q), while the narrower component (with a typically smaller C_Q) results from Sc with H_2O attached. This assignment is supported by simple density functional theory (DFT) calculations on isolated trimer units (using the CASTEP code),[43,44] where larger quadrupolar coupling values are observed for Sc–OH species (Supporting Information). Figure 3 shows that when the scandium content is low, a greater proportion of the Sc appears to be associated with Sc–OH species, indicating preferential substitution of Al into sites with coordinated water molecules. Figure 4 shows ^{13}C CP MAS NMR spectra of the MIL-100(Sc,Al) compounds. In general, the ^{13}C spectra are similar to those in the literature for the Sc and Al pure end members,[34,42] but exhibit different relative intensities in the carboxylate C region between 168–175 ppm. Each carboxylate linker is bonded via O atoms to two of the metal centres of a trimer, each of which may be Sc or Al. DFT calculations of the expected chemical shifts of different compositions of isolated model trimers using the CASTEP code[43,44] indicates a clear 2–3 ppm shift of the carboxyl C species to lower chemical shift for (Al,Sc) and (Al,Al) pairs compared to (Sc,Sc) next-nearest-neighbour environments, but suggests that unambiguous differentiation between (Al,Sc) and (Al,Al) environments is not possible. On the basis of the experimental and calculated NMR parameters, it is therefore possible to confirm the inclusion of Al in trimers in MIL-100(Sc,Al), but it is not possible to differentiate unambiguously between the inclusion of Al in mixed Al_nSc_{3-n} trimers or as Al_3 trimers.

For the MIL-100(Sc,Fe) series of materials, evidence for the incorporation of Fe^{3+} in the trimers in place of Sc^{3+} was obtained by diffuse reflectance UV/Vis and X-ray absorption spec-

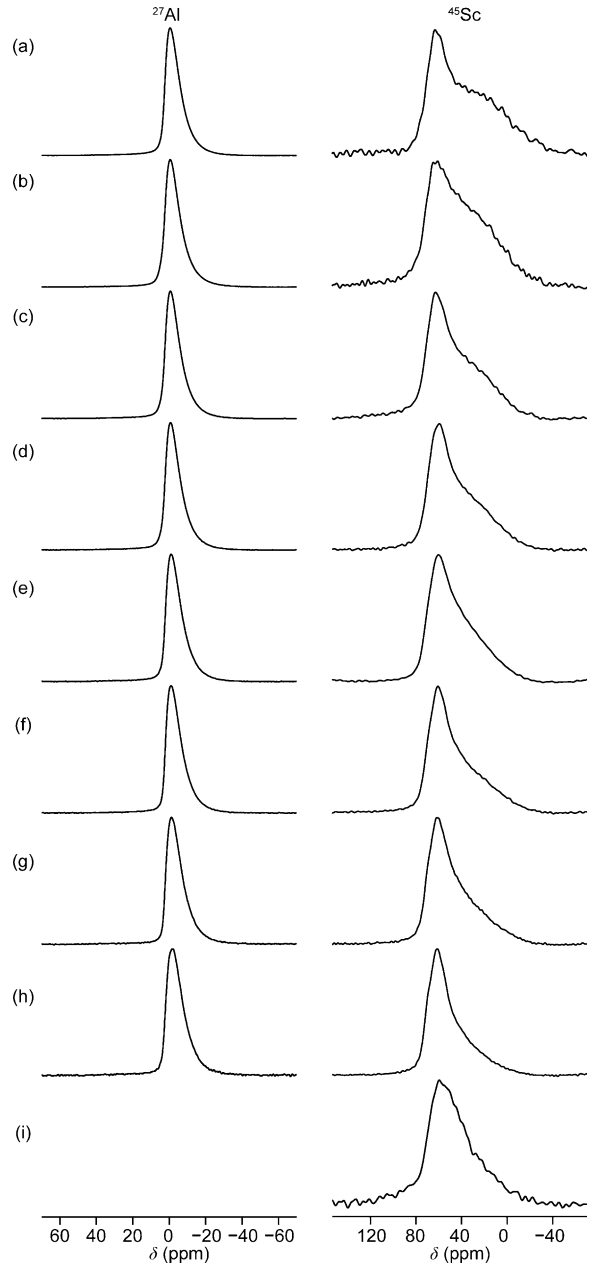

Figure 3. ^{27}Al (left) and ^{45}Sc (right) MAS NMR spectra (14.1 T) of MIL-100(Sc,Al) samples a) $Sc_{10}Al_{90}$, b) $Sc_{20}Al_{40}$, c) $Sc_{30}Al_{70}$, d) $Sc_{40}Al_{60}$, e) $Sc_{50}Al_{50}$, f) $Sc_{60}Al_{40}$, g) $Sc_{70}Al_{30}$, h) $Sc_{80}Al_{20}$, and i) Sc_{100}. Spectra were recorded at MAS rates of 14 (^{27}Al) and 20–30 kHz (^{45}Sc).

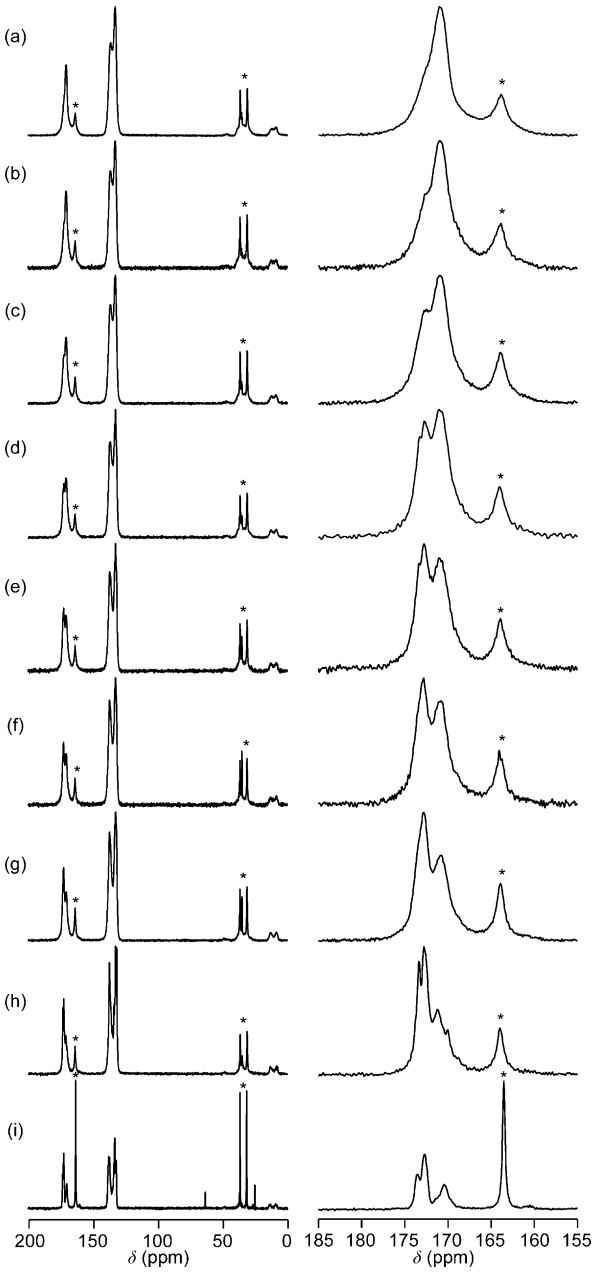

Figure 4. ^{13}C CP MAS NMR spectra (9.4 T) of MIL-100(Sc,Al) a) $Sc_{10}Al_{90}$, b) $Sc_{20}Al_{40}$, c) $Sc_{30}Al_{70}$, d) $Sc_{40}Al_{60}$, e) $Sc_{50}Al_{50}$, f) $Sc_{60}Al_{40}$, g) $Sc_{70}Al_{30}$, h) $Sc_{80}Al_{20}$, and i) Sc_{100}. Spectra were recorded with a MAS rate of 12.5 kHz. Asterisk indicates residual solvent.

troscopy, the latter performed at beamline B18 of the Diamond Light Source Synchrotron.[45] Fe K-edge X-ray absorption data were normalised to the edge step in the program Athena to yield X-ray absorption near-edge (XANES) spectra and background subtracted extended X-ray absorption fine structure (EXAFS) spectra.[46] The k^3-weighted EXAFS spectra were analysed using Artemis,[47] which implements the FEFF code and uses the IFEFFIT EXAFS library,[48] with coordination numbers of atomic shells fixed at expected values, and shell distances and thermal parameters (σ^2) were refined along with E_0 (threshold energy) and $S_0{}^2$ (amplitude reduction factor). The goodness of fit is reported as the R-factor [Equation (1)]:

$$R_f = \sum_i^{\text{Nfit}} \left[\chi_i^{\text{data}} - \chi_i^{\text{model}}(x)\right]^2 / \sum_i^{\text{Nfit}} \left[\chi_i^{\text{data}}\right]^2 \quad (1)$$

where χ_i^{data} and χ_i^{model} are the i^{th} absorption coefficient point of the data and model, respectively. The errors reported on EXAFS parameters are purely statistical. UV/Vis spectra of the series of materials shows increasing absorbance with maxima at 450–600 nm, characteristic of 3d–3d transitions of octahedral $Fe^{III}O_6$ (Figure 5).

This assignment was confirmed by X-ray absorption spectroscopy, where Fe K-edge spectra of the MIL-100(Sc,Fe) series (obtained by background subtraction) were compared with

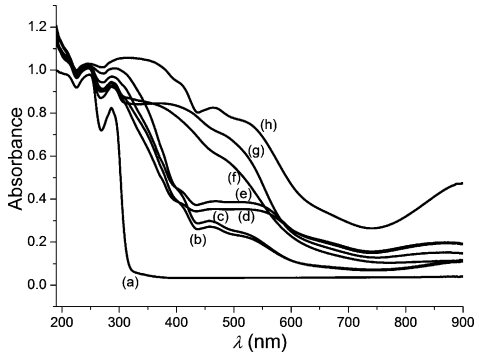

Figure 5. UV/Vis spectroscopy of a) MIL-100(Sc), b) MIL-100($Sc_{80}Fe_{20}$), c) MIL-100($Sc_{60}Fe_{40}$), d) MIL-100($Sc_{40}Fe_{60}$), e) MIL-100($Sc_{20}Fe_{80}$), f) MIL-100($Sc_{80}Fe_{20}$)XS, g) MIL-100($Sc_{60}Fe_{40}$)XS, and h) MIL-100(Fe).

the standards $FeCl_2{\cdot}4H_2O$ (Fe^{II}), Fe_3O_4 (magnetite) (average oxidation state of 2.67), and α-Fe_2O_3, hematite (Fe^{III}). As expected, there is a shift in edge position to higher energy from Fe^{II} to $Fe^{2.67}$ to Fe^{III} in the standards.[47] The K-edge energy and XANES of Fe in the MIL-100(Sc,Fe) samples (Figure 6) are characteristic of Fe^{III} in an octahedral environment, shifted to a slightly higher energy relative to α-Fe_2O_3 as a result of the very different local coordination environment of Fe^{III} in the trimeric clusters. Similar Fe K edge XANES spectra have been observed for MIL-100(Fe) previously.[49]

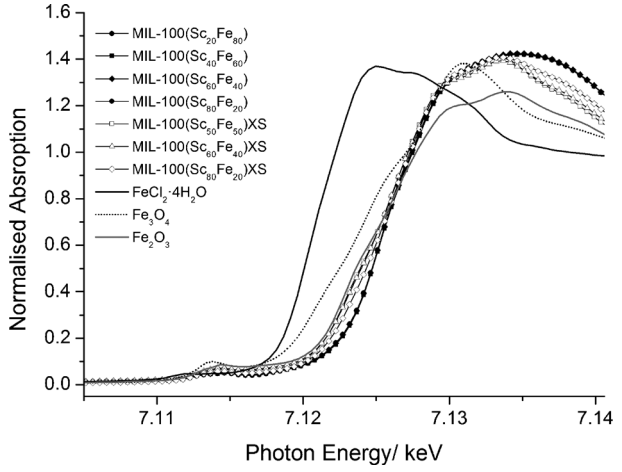

Figure 6. Fe K-edge XANES spectra of MIL-100(Sc,Fe) and MIL-100(Sc,Fe)XS materials, compared with XANES of standards $FeCl_2{\cdot}4H_2O$, Fe_3O_4, and α-Fe_2O_3.

EXAFS spectra ($k = 2.5$–12.0 Å^{-1}) were modelled based on the published crystal structure of MIL-100(Cr),[36] with four shells of atoms and the Cr sites replaced by appropriate metals as next-nearest neighbours. For each sample, two models were tested, one in which the Fe^{3+} atom had two Fe^{3+} next-nearest neighbours in the trimer, and one in which the Fe^{3+} had two Sc^{3+} nearest neighbours. The samples all gave similar EXAFS spectra, and both models gave reasonable fits, with all of the Fe–M intra-trimer distances of circa 3.36 Å, but slightly more realistic parameters were obtained with a model of Fe_3 trimers, suggesting there is limited mixing of Sc^{3+} and Fe^{3+} in the trimers in the material. The final details for MIL-100($Sc_{80}Fe_{20}$) are given in Table 2 as an example, and the fit is shown in Figure 7. Additional data are given in the Supporting Information, Section S5. The unit cell parameter determined by Le Bail analysis of PXRD data (Figure 2) showed a trend of decreasing length with increasing Fe^{3+} content, which is expected because the ionic radius of high-spin Fe^{3+} (0.645 Å) is smaller than that of Sc^{3+} (0.745 Å) and so the average unit cell size

Table 2. Modelled coordination shells of Fe in MIL-100($Sc_{80}Fe_{20}$) consistent with an environment of $Fe_3O(OR)_3(O_2C)_6$ trimers used to fit k^3-weighted Fe K-edge EXAFS.[a]

Shell	*N*	*R* [Å]	σ^2 [Å^2]
O	6	2.005 ± 0.012	0.0087 ± 0.0019
C	4	3.013 ± 0.062	0.0094 ± 0.0090
O	4	3.273 ± 0.184	0.0172 ± 0.0244
Fe	2	3.352 ± 0.071	0.0116 ± 0.0081

[a] $E_0 = 0.48$, $S_0^2 = 0.96$, and $R_f = 0.051$.

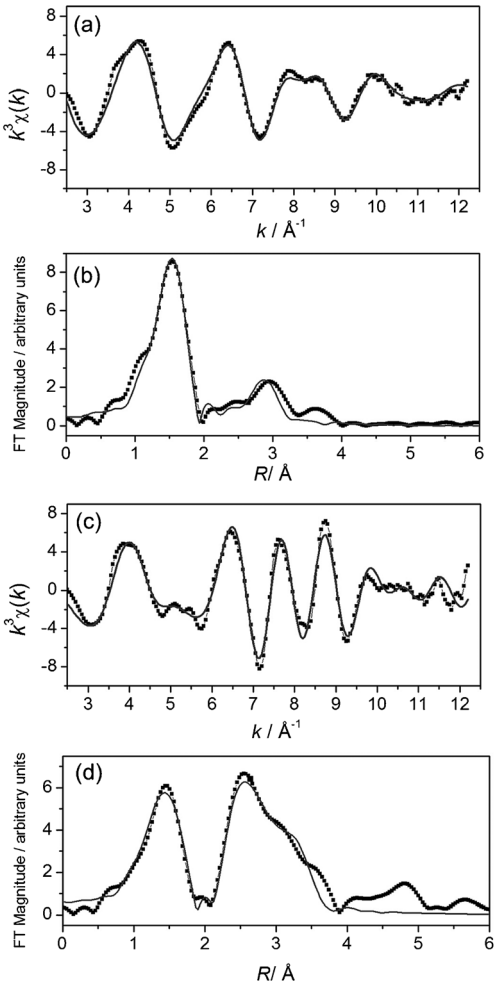

Figure 7. a) Fitted k^3-weighted EXAFS spectrum of MIL-100($Sc_{80}Fe_{20}$) with b) the magnitude of its Fourier transform and c) Fitted k^3-weighted EXAFS spectrum of MIL-100($Sc_{50}Fe_{50}$)XS, with d) the magnitude of its Fourier transform. ■ measured data, —— fitted function.

should decrease as the concentration of Fe^{3+} in the trimers or the fraction of Fe_3 trimers increased.

A sample of methanol-washed MIL-100(Sc) was analysed by TGA in flowing air. The results are consistent with the treated solid having a formula $Sc_3O(MeOH)_2(MeO)(BTC)_2{\cdot}1.68\,DMF$ (although it may be that some of the DMF molecules are coordinated to Sc^{3+} cations in place of MeOH), with 14 wt% solvent and a final residue of Sc_2O_3 of 26% of the "dried" material. The residual mass of the MIL-100(Sc,Fe) samples increased as the Fe content increased, in line with the higher atomic weight of Fe (ending up as Fe_2O_3 at high temperatures). Furthermore, the thermal stability of the solids decreased as Fe was included, so that whereas weight loss from MIL-100(Sc) was essentially complete by 823 K, MIL-100(Fe) had fully decomposed by 673 K. The N_2 adsorption isotherms (Supporting Information, Figure S6.1) of indicated all samples had similar porosities, with pore volumes of about 0.93 $cm^3\,g^{-1}$.

In the MIL-100(Sc,Fe)-XS series of materials prepared with excess trivalent metal salts in the synthesis, the samples are a characteristic pink colour, rather than the orange of the MIL-100(Sc,Fe) solids. The UV/Vis spectra (Figure 5) show a strong absorption band from 300–600 nm with a distinctive distribution of maxima that is different from MIL-100(Fe). X-ray absorption spectroscopy on these samples indicated the iron was trivalent, but in a mixture of environments. Comparison of the XANES of these samples with those of α-Fe_2O_3 (hematite) and MIL-100(Sc,Fe) suggests at least part of the Fe^{3+} is present as α-Fe_2O_3 (Figure 6), with the remainder in trimer units and therefore giving the same XANES spectral form as Fe in the MIL-100(Sc,Fe) series. As the Fe:Sc molar ratio increases the contribution of the α-Fe_2O_3 increases. No sharp diffraction peaks for α-Fe_2O_3 are observed in the PXRD, indicating it must be present in nanocrystalline form. The EXAFS spectra also show the presence of α-Fe_2O_3 in the "XS" samples. All show higher shell intensity (>2.5 Å in the Fourier transforms) that is much closer to the data of α-Fe_2O_3 than to those of MIL-100(Sc,Fe), and the EXAFS data cannot be fitted with the MIL-100 models that fitted the Fe EXAFS for the MIL-100(Sc,Fe) series. For the sample with the highest Fe content (MIL-100($Sc_{50}Fe_{50}$)XS, the EXAFS can be fitted satisfactorily using coordination numbers and distances from a model that is based on a 1:1 mixture of α-Fe_2O_3 and MIL-100(Fe) (Figure 7 and Table 3).

Visually, the ratio of the intensity of the higher coordination shell peaks characteristic of α-Fe_2O_3 to that of the first coordination shell (there are six Fe–O distances of around 1.98 Å for Fe in both trimer sites in MIL-100 and in α-Fe_2O_3) decreases as the amount of Fe in the XS samples decreases (Figure 8), suggesting that at low Fe contents there is a lower fraction of Fe in α-Fe_2O_3 nanoparticles compared to trimer Fe.

Attempts to quantify the relative amounts of Fe in trimer and α-Fe_2O_3 sites from the EXAFS analysis are not straightforward; however, because there is considerable overlap in the position of shells, and the apparent coordination number of atoms in nanoparticles will depend in part on their size. Nevertheless, a simple 1:1 model of Fe in the two types of sites is found to be a better fit to the MIL-100($Sc_{80}Fe_{20}$)XS EXAFS than

Table 3. Modelled coordination shells of Fe in MIL-100($Sc_{50}Fe_{50}$)XS consistent with an α-Fe_2O_3 and MIL-100(Fe) mixture used to fit k^3-weighted Fe K-edge EXAFS.[a]

Shell	N	R [Å]	σ^2 [Å^2]
O	6	1.970 ± 0.023	0.0132 ± 0.0038
Fe	2	2.935 ± 0.019	0.0049 ± 0.0024
Fe	2.5	3.352 ± 0.025	0.0060 ± 0.0032
Fe	3	3.682 ± 0.025	0.0082 ± 0.0030

[a] $E_0 = -5.18$, $S_0^2 = 1.03$, and $R_f = 0.11$.

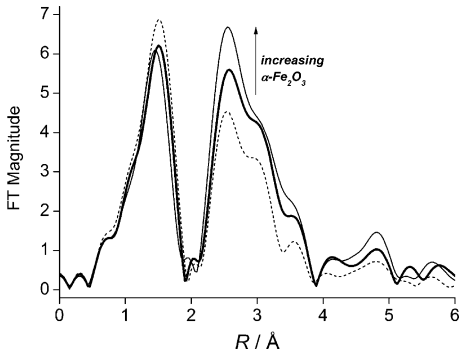

Figure 8. Fourier transform magnitudes of EXAFS spectra of MIL-100($Sc_{80}Fe_{20}$)XS (-----), MIL-100($Sc_{60}Fe_{40}$)XS (——), and MIL-100($Sc_{50}Fe_{50}$)XS (——) materials, showing increasing intensity in higher shells characteristic of α-Fe_2O_3.

the α-Fe_2O_3 model, and the simplest interpretation of the XS series of samples is of a system with some Fe substitution in trimer sites and a strong component of nanocrystalline α-Fe_2O_3 that increases as Fe levels increase (Supporting Information, Section S5). Indeed, TGA analysis of the MIL-100(Sc,Fe)XS materials show higher residual mass than standard MIL-100(Sc,Fe) samples of similar Sc:Fe ratios, which can be attributed to the presence of α-Fe_2O_3 in the as-prepared MOF, which adds into the total Sc_2O_3 and Fe_2O_3 formed upon calcination. Increasing Fe contents also result in lower thermal stability compared to the pure MIL-100(Sc), which suggests that at least some of the Fe substitutes into trimer sites in the MOF framework. This is supported by the observed reduction of the unit cell size as the iron content increases, although this effect is less than that observed for the MIL-100(Sc,Fe) series, because only a portion of the Fe substitutes into the trimer sites. For the MIL-100($Sc_{60}Fe_{40}$)XS sample, for example, the TGA gives a residual TGA mass of 38 wt%. Assuming one in four of the trimer sites is occupied by Fe (estimated from the unit cell constant), and that the solid has a similar residual DMF content to that of MIL-100(Sc), the overall composition can be estimated as $Sc_{2.4}Fe_{0.6}O(MeOH)_2(MeO)(BTC)_2{\cdot}1.68\,DMF{\cdot}z\,Fe_2O_3$. The residual mass can then be accounted for if $z = 0.9$ in this formula. In this case most of the Fe in the sample (ca. 75%) is present as α-Fe_2O_3 nanoparticles, in broad agreement with the EXAFS analysis.

Transmission electron microscopy of MIL-100($Sc_{60}Fe_{40}$)XS confirmed that there were no large particles of iron oxide in the hybrid material. Although the material is highly beam sen-

sitive, high magnification images show that for some MIL-100 particles, but not all, associated nanoparticles a few nm in size are visible (Supporting Information, Figure S7.1). This suggests that some iron oxide is present as nanoparticles too large to fit in perfectly crystalline MIL-100, but it is not clear if these are at the surface or embedded or how much of the total α-Fe_2O_3 content they represent.

The N_2 adsorption (Figure 9) shows a sharp reduction in specific pore volume with increasing Fe content that is due to the presence of α-Fe_2O_3. Most of this decrease is simply a result of

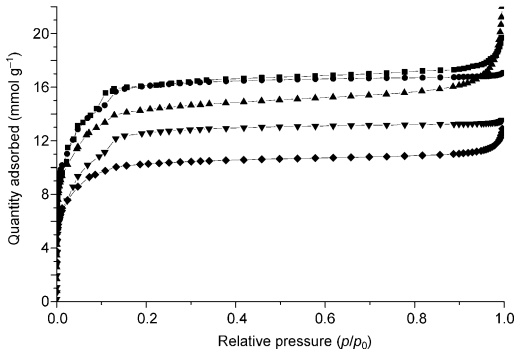

Figure 9. N_2 adsorption at 77 K (not offset) of MIL-100(Sc) (■), MIL-100($Sc_{90}Fe_{10}$)XS (●), MIL-100($Sc_{80}Fe_{20}$)XS (▲), MIL-100($Sc_{60}Fe_{40}$)XS (▼), and MIL-100($Sc_{50}Fe_{50}$)XS (◆).

the additional mass of the non-porous α-Fe_2O_3, but some reduction owing to the presence of the iron oxide species within the pores (rather than on the external surface) is also likely (Supporting Information). That the PXRD patterns of MIL-100(Sc,Fe)XS materials show distinct differences from the MIL-100(Sc,M) materials in the intensities of some low angle diffraction peaks (Supporting Information, Figure S1.2) also indicates that at least some of the nanoparticles are within the cages of the MIL-100 structure. The nature of this composite is therefore significantly different from that of the Fe_3O_4@ZIF-8 composite prepared by Faustini et al., where the iron oxide particles exist in their own phase on the surface of ZIF-8 particles and give a separate PXRD pattern.[50]

Catalysis

Lewis acidic catalysis

The catalytic performance of these materials was first examined in a series of Lewis acid catalysed reactions. Prior to this, optimum conditions were determined for the removal of DMF molecules included within the pores of MIL-100(Sc) during synthesis without damaging the framework. MIL-100(Sc) treated in different ways was examined by IR active molecular probes for Lewis acid sites, CD_3CN, and CO.[51–53] As-prepared MIL-100(Sc) was activated by prolonged washing with methanol before being heated under vacuum at 423 K and then at 523 K. Infrared spectroscopic analysis showed that some DMF from the synthesis remained in the pores even after washing, which is possibly strongly bound to Sc^{3+} sites, as shown by the presence of absorption bands at 2945 and 2873 cm^{-1} (Figure 10).

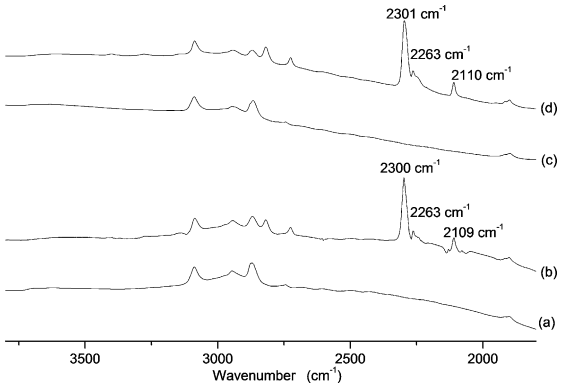

Figure 10. IR spectra before and after CD_3CN dosing on both as-prepared and methanol-activated MIL-100(Sc). a) As-prepared MIL-100(Sc) heated to 523 K, b) after CD_3CN dosing; c) methanol-activated MIL-100(Sc) heated to 523 K, d) after CD_3CN dosing.

Dosing of CD_3CN at room temperature onto the methanol-activated MIL-100(Sc), evacuated at 523 K, gave an absorption band at 2301 cm^{-1}, a blue shift of 38 cm^{-1} from that in the unperturbed liquid-like CD_3CN in the pores (2263 cm^{-1}), indicating the presence of acid sites that can be assigned as coordinatively unsaturated Sc^{3+} cations (Figure 10). Normally blue shifts arise for C≡N interacting with acid sites, both Lewis and Brønsted. Although the shift of the C≡N bond frequency upon adsorption was much lower than for the bands observed upon adsorption on MIL-100(Al) (band at 2321 cm^{-1}),[53] it was similar to that of MIL-100(Cr) (band at 2305 cm^{-1})[51] and MIL-100(Fe) (band at 2304 cm^{-1}).[52] This suggests that the Lewis acid strength of the MIL-100(Al) is the highest of the solids examined.

To investigate further the presence of Lewis acid sites in MIL-100(Sc), quantitative CO adsorption/IR spectroscopy was performed at 77 K. CO adsorbed on MIL-100(Sc) treated with methanol and activated at 423 K, and cooled to 77 K gave an absorption band at 2180 cm^{-1} (similar to that reported previously for CO on MIL-100(Sc),[54] 42 cm^{-1} blue-shifted compared to unperturbed CO and characteristic of adsorption at Lewis acid sites (Supporting Information, Figure S8.3). Quantification indicated a Lewis acid concentration of 0.82 mmol g^{-1} (Supporting Information, Section S8). Using slightly different activation conditions MIL-100(Cr) has 2.6 mmol g^{-1} (absorption frequency ca. 2190 cm^{-1}), MIL-100(Fe) 1.94 mmol g^{-1} (absorption frequency 2180 cm^{-1}) and MIL-100(Al) 2.2 mmol g^{-1} (2183 cm^{-1}).[51–53] When activated at 523 K the amount of Lewis acidic sites increased to 1.96 mmol g^{-1} (equivalent to 1.5 Lewis acid sites per trimer) compared to MIL-100(Cr), 3.41 mmol g^{-1} sites and MIL-100(Fe), 3.66 mmol g^{-1} (equivalent to two Lewis acid sites per trimer). However, subsequent examination of MIL-100(Sc) catalysts activated at 423 and 523 K in the carbonyl ene reaction showed that activation at 523 K did not improve the catalytic performance. Instead, lower selectivity and the generation of unwanted by-products was observed, which is possibly due to the generation of unwanted defect sites. Indeed, the higher activation temperature was found to result in reduction of pore volume, as measured by N_2 adsorption at

77 K, to 0.55 $cm^3 g^{-1}$, suggesting partial degradation of the structure. Consequently, methanol washing followed by activation at 423 K was chosen as the standard activation procedure for all scandium-based MIL-100 materials.

Our first catalytic objective was to investigate whether the Sc/Al, Sc/Cr and Sc/Fe MOFs would still perform well as Lewis acid catalysts. We first investigated activity in the carbonyl ene reaction of α-methylstyrene with ethyl trifluoropyruvate to form ethyl-2-hydroxy-4-phenyl-2-(trifluoromethyl)pent-4-enoate (Scheme 1).[55]

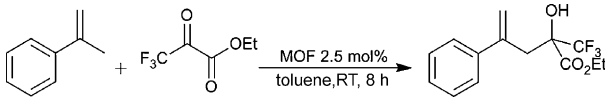

Scheme 1. Carbonyl ene reaction of α-methylstyrene with ethyl trifluoropyruvate.

Results are given in Figure 11 and the Supporting Information, Table S9.2.1. For the MIL-100(Sc,Al) system, the substitution of Al for Sc resulted in a strong decrease of the activity, with conversion dropping from 99 to 30% as Al is substituted

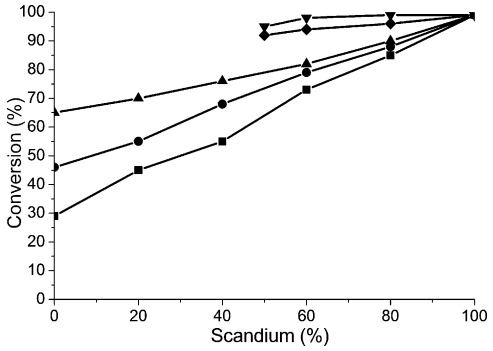

Figure 11. Percentage conversion after 6 h in the reaction of α-methylstyrene with ethyl trifluoropyruvate catalysed by the following series of materials: MIL-100(Sc,Fe)XS (▼), MIL-100(Sc,Fe)XS (mass adjusted on basis of metal content; see text, ◆), MIL-100(Sc,Cr) (▲), MIL-100(Sc,Fe) (●), and MIL-100(Sc,Al) (■).

for Sc to full MIL-100(Al), even though the apparent Lewis acid strength, as inferred from the reported IR frequency of adsorbed CO on the Al^{3+} sites, is higher for MIL-100(Al) than for MIL-100(Sc). The same trend of decreasing activity with decreasing Sc^{3+} content in the carbonyl ene reaction is observed for the MIL-100(Sc,Cr) and the MIL-100(Sc,Fe) samples, where the order of activity decreases according to the added trivalent metal in the order Sc > Cr > Fe > Al (Figure 11). Our previous studies had shown that MIL-100(Sc) was a fully heterogeneous catalyst under these conditions, so that removal by filtration reduced the reaction rate to background levels.[35]

Similar trends in catalytic activity, Sc > Cr > Fe > Al, were observed for MIL-100(Sc,M) (M = Cr, Fe, Al) solids in the conjugate addition of indoles to 2-methyl vinyl ketone (Scheme 2; Supporting Information, Table S9.3.1). Catalysed syntheses over

Scheme 2. Conjugate addition of 2-methylindole to methyl vinyl ketone.

MOFs involving nitrogen-containing heterocyclic compounds are of widespread interest, as recently summarised.[56]

These results show that no straightforward correlation can be drawn between measurement of Lewis acidity by probe Lewis bases adsorbed from the gas phase and the activity in Lewis acid catalysis in solution. It is likely that, compared to Sc^{3+}, the Cr^{3+}, Fe^{3+}, and especially Al^{3+} cations bind intermediates or products of the reaction too strongly, inhibiting the reaction.

For the MIL-100(Sc,Fe)XS samples the presence of nanoparticulate α-Fe_2O_3 enhances the specific activity of the Lewis acid catalyst (so that a MIL-100($Sc_{60}Fe_{40}$)-XS material is as active per gram as MIL-100(Sc). It was also possible to scale the amounts of added catalyst so that they contained the same mass of metal as the corresponding MIL-100(Sc,Fe) materials, by comparing the residual masses of samples in TGA experiments. In these experiments, the activities decreased slightly compared to MIL-100(Sc) but remained higher than for MIL-100(Sc,Fe) catalysts: Fe in supported α-Fe_2O_3 nanoparticles is a better Lewis acid catalyst than Fe in trimer sites.

Bifunctional catalysis

Given the activity of these MIL-100 materials in Lewis acid catalysis, our next step was to investigate those that contained scandium and iron for their ability to perform bifunctional Lewis acid-oxidation catalysis, because iron-based MOFs are known to promote oxidation reactions.[37] The Lewis acid-catalysed tandem Friedel–Crafts addition reaction between 2-methylindole and trifluoroacetaldehyde ethyl hemiacetal followed by oxidation of the product (Scheme 3) was chosen as a target tandem reaction requiring bifunctionality.

For the initial, Lewis acid-catalysed step (Scheme 4), MIL-100(Sc) is a far superior catalyst to HKUST-1(Cu) or MIL-100(Fe)

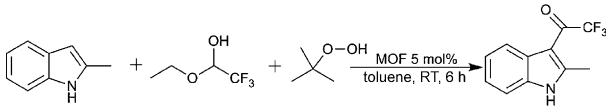

Scheme 3. Tandem Friedel–Crafts addition and oxidation reaction of 2-methylindole with trifluoroacetaldehyde ethyl hemiacetal and *tert*-butyl hydroperoxide.

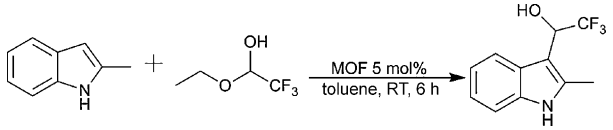

Scheme 4. Friedel–Crafts addition of trifluoroacetaldehyde ethyl hemiacetal to 2-methylindole.

(Table 4). Whereas HKUST-1(Cu) may be disadvantaged in terms of both active site electronic and window size steric effects (smaller window size),[35] the Fe^{3+} sites in MIL-100(Fe) are clearly less active Lewis acid sites for the reaction than Sc^{3+}. Straightforward replacement of Sc by cheaper Fe in the MIL-100(Sc,Fe) materials therefore results in a reduction of activity, but replacement of 40% of Sc^{3+} with Fe^{3+} still gives an active catalyst (78% conversion after 6 h at 5 mol% MIL-100(Sc,Fe) load, increasing to >99% after 16 h).

Friedel–Crafts addition of trifluoroacetaldehyde ethyl hemiacetal to indole, *N*-methylindole, pyrrole, and dimethoxybenzene was also achieved using this catalyst system. For all of these reactions, using an equivalent mass of MIL-100($Sc_{60}Fe_{40}$)XS material gave slightly higher conversions than the pure MIL-100(Sc) material and outperformed MIL-100 with a similar Sc/Fe ratio, but with all of its iron present in the trimers.

The activity of the Fe-bearing MIL-100 materials was then investigated in the oxidation of the alcohol addition products formed in the reactions described above, according to reactions of the type shown in Scheme 5.

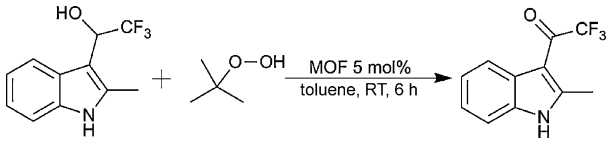

Scheme 5. Oxidation of 2,2,2-trifluoro-1-(2-methyl-1H-indol-3-yl)ethanol using *tert*-butyl hydroperoxide.

The results in Table 5 show that while MIL-100(Sc) and HKUST-1(Cu) are poor catalysts for this reaction (entries 2 and 17) the Fe-containing MOFs have significant activity, and in the mixed MIL-100(Sc,Fe) materials there is good activity even at Fe contents as low as 40 mol%. To confirm the catalysis was heterogeneous, and did not result from Fe species leached from the MIL-100, a sample of MIL-100($Sc_{60}Fe_{40}$) was used in the oxidation reaction described in Table 5 and removed by filtration after 3 h. The catalytic conversion then remained at 58% for 24 h.

Having shown that mixed-metal MIL-100(Sc,Fe) materials catalyse the deacetalisation–addition reaction and oxidation reactions separately, we next investigated combining the sequential deacetalisation, Friedel–Crafts addition and oxidation into a one-pot procedure with all reagents added at the start (Tables 6 and 7). While in some respects a relatively simple tandem reaction, this involves carrying out a catalytic C–C bond-forming reaction on an aldehyde intermediate under strongly oxidizing conditions, so from the outset we analysed for trifluoroacetic acid, expecting to see it as a by-product. It was therefore encouraging to find that, particularly using the MIL-100($Sc_{60}Fe_{40}$) catalyst, a very clean tandem deacetalisation–Friedel–Crafts addition–oxidation occurs, using just 1.2 equivalents of trifluoroacetaldehyde ethyl hemiacetal (Table 6, Entry 4). Remarkably, no trifluoroacetic acid was detected by $^{19}F\{^1H\}$ NMR spectroscopic monitoring of the reaction mixture.

Table 4. Friedel–Crafts reactions of 2-methylindole and related compounds with trifluoroacetaldehyde ethyl hemiacetal.[a]

Entry	MOF	Substrate	Product	Product [%][b]
1	No catalyst	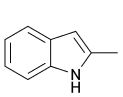	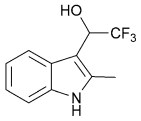	19
2	MIL-100(Sc)			98
3	MIL-100($Sc_{80}Fe_{20}$)			89
4	MIL-100($Sc_{60}Fe_{40}$)			78
5	MIL-100($Sc_{60}Fe_{40}$)[c]			>99
6	MIL-100($Sc_{60}Fe_{40}$)[d]			78
7	MIL-100($Sc_{60}Fe_{40}$)			69
8	MIL-100($Sc_{20}Fe_{80}$)			62
9	MIL-100($Sc_{80}Fe_{20}$)XS			99(98)
10	MIL-100($Sc_{60}Fe_{40}$)XS			99(96)
11	MIL-100($Sc_{50}Fe_{50}$)XS			90(89)
12	MIL-100(Fe)			55
13	HKUST-1(Cu)			28
14	No catalyst		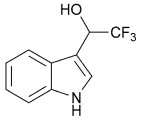	12
15	MIL-100(Sc)			90
16	MIL-100($Sc_{60}Fe_{40}$)			80
17	MIL-100($Sc_{60}Fe_{40}$)XS			95
18	MIL-100(Fe)			45
19	HKUST-1(Cu)			22
20	No catalyst		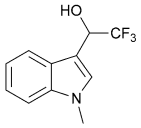	15
21	MIL-100(Sc)			89
22	MIL-100($Sc_{60}Fe_{40}$)			78
23	MIL-100($Sc_{60}Fe_{40}$)XS			91
24	MIL-100(Fe)			50
25	No catalyst		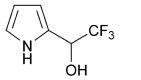	8(3:1)
26	MIL-100(Sc)			99 (7:1)
27	MIL-100($Sc_{60}Fe_{40}$)			80(9:1)
28	MIL-100($Sc_{60}Fe_{40}$)XS			99(9:1)
29	MIL-100(Fe)			43(8:1)
26	No catalyst	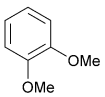	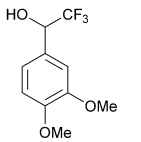	0
27	MIL-100(Sc)			50
28	MIL-100($Sc_{60}Fe_{40}$)			40
29	MIL-100($Sc_{60}Fe_{40}$)XS			56
30	MIL-100(Fe)			19
31	HKUST-1(Cu)			0

[a] See Scheme 4. Reactions carried out using 1 mmol of 2-methylindole and 1.2 mmol trifluoroacetaldehyde ethyl hemiacetal in 5 mL toluene: 5 mol% MOF (metal cation/substrate), at room temperature for 6 h unless otherwise stated. [b] Determined by $^{19}F\{^1H\}$ NMR using 1-fluoronaphthalene as internal standard; ^1H NMR also measured. [c] Reaction time 16 h. [d] Recycled MIL-100. Reactions 26–31 carried out at 90 °C for 16 h.

In fact, the tandem reaction delivers ketone more effectively than performing the oxidation directly on the isolated secondary alcohol. A possible cause of this is that the secondary alcohol (the intermediate in the reaction) might diffuse more slowly into the pores of the MOF than the reactant indole, and this diffusion step could be removed by generating the intermediate in situ from the indole. Experimental measurement of

Table 5. Oxidation of 2,2,2-trifluoro-1-(2-methyl-1H-indol-3-yl)ethanol and related compounds.[a]

Entry	MOF	Substrate	Product [%][b]
1	No catalyst	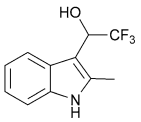	0
2	MIL-100(Sc)		8
3	MIL-100($Sc_{80}Fe_{20}$)		48
4	MIL-100($Sc_{60}Fe_{40}$)		80
5	MIL-100($Sc_{60}Fe_{40}$)[c]		79
6	MIL-100($Sc_{60}Fe_{40}$)[d]		90
7	MIL-100($Sc_{60}Fe_{40}$)[e]		>99
8	MIL-100($Sc_{60}Fe_{40}$)[f]		77
9	MIL-100($Sc_{60}Fe_{40}$)[g]		76
10	MIL-100($Sc_{60}Fe_{40}$)[h]		81
11	MIL-100($Sc_{40}Fe_{60}$)		81
12	MIL-100($Sc_{20}Fe_{80}$)		84
13	MIL-100($Sc_{80}Fe_{20}$)XS		57(56)
14	MIL-100($Sc_{60}Fe_{40}$)XS		70(70)
15	MIL-100($Sc_{50}Fe_{50}$)XS		74(72)
16	MIL-100(Fe)		85
17	HKUST-1(Cu)		9
18	No catalyst	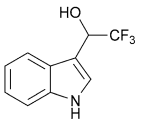	0
19	MIL-100(Sc)		11
20	MIL-100($Sc_{60}Fe_{40}$)		76
21	MIL-100($Sc_{60}Fe_{40}$)XS		72
22	MIL-100(Fe)		80
23	HKUST-1(Cu)		9
24	No catalyst	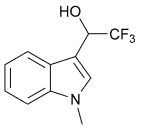	0
25	MIL-100(Sc)		6
26	MIL-100($Sc_{60}Fe_{40}$)		70
27	MIL-100($Sc_{60}Fe_{40}$)XS		65
28	MIL-100(Fe)		78
29	No catalyst	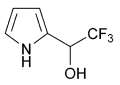	0
30	MIL-100(Sc)		11
31	MIL-100($Sc_{60}Fe_{40}$)		95
32	MIL-100($Sc_{60}Fe_{40}$)XS		92
33	MIL-100(Fe)		96
34	No catalyst	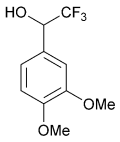	0
35	MIL-100(Sc)		8
36	MIL-100($Sc_{60}Fe_{40}$)		90
37	MIL-100($Sc_{60}Fe_{40}$)XS		80
38	MIL-100(Fe)		91
39	HKUST-1(Cu)		65

[a] See Scheme 5 for example reaction. Reactions carried out using 1 mmol of 2,2,2-trifluoro-1-(2-methyl-1*H*-indol-3-yl)ethanol and 4 mmol *tert*-butyl hydroperoxide in 5 mL toluene/decene and stirred at room temperature for 6 h unless otherwise stated: 5 mol% MOF. [b] Determined by $^{19}F\{^1H\}$ NMR using 1-fluoronaphthalene as internal standard. ^1H NMR also measured. [c] Recycled MIL-100. [d] Alcohol substrate given 1 h incubation period before *tert*-butyl hydroperoxide is added. [e] Stirred at room temperature for 16 h. [f] Volume of solvent doubled, [g] tripled, [h] halved. Reactions 34–39 carried out at 90 °C for 16 h.

the rate of uptake of 2-methylindole and 2,2,2-trifluoro-1-(2-methyl-1-indol-3-yl)ethanol showed that the "intermediate" secondary alcohol indeed diffused more slowly into the pores of MIL-100($Sc_{60}Fe_{40}$) than 2-methylindole. Indeed, for the alcohol oxidation allowing the alcohol one hour to adsorb before starting the reaction increases the overall conversion to product (Table 5, entry 6).

Table 6. One-pot tandem reaction of 2-methylindole with trifluoroacetaldehyde ethyl hemiacetal and tert-butyl hydroperoxide using various MOF catalysts.[a]

Entry	MOF	Product [%][b]
1	No catalyst	0
2	MIL-100(Sc)	10
3	MIL-100($Sc_{80}Fe_{20}$)	55
4	MIL-100($Sc_{60}Fe_{40}$)	96
5	MIL-100($Sc_{60}Fe_{40}$)[c]	96
6	MIL-100($Sc_{60}Fe_{40}$)[d]	95
7	MIL-100($Sc_{60}Fe_{40}$)[e]	96
8	MIL-100($Sc_{60}Fe_{40}$)[f]	95
9	MIL-100($Sc_{60}Fe_{40}$)	78
10	MIL-100($Sc_{20}Fe_{80}$)	67
11	MIL-100($Sc_{80}Fe_{20}$)XS	90(88)
12	MIL-100($Sc_{60}Fe_{40}$)XS	94(90)
13	MIL-100($Sc_{50}Fe_{50}$)XS	89(85)
14	MIL-100(Fe)	60
15	HKUST-1(Cu)	12

[a] See Scheme 3. Reactions carried out using 1 mmol of 2-methylindole and 1.2 mmol trifluoroacetaldehyde ethyl hemiacetal and 4 mmol *tert*-butyl hydroperoxide in 5 mL toluene/decene at room temperature for 6 h. [b] Determined by $^{19}F\{^1H\}$ NMR using 1-fluoronaphthalene as an internal standard; ^1H also measured. [c] Recycled MIL-100($Sc_{60}Fe_{40}$). [d] Concentration of solvent doubled, [e] tripled, [f] halved.

Table 7. One-pot tandem reaction of indole and related compounds with trifluoroacetaldehyde ethyl hemiacetal and tert-butyl hydroperoxide using various MOF catalysts (Scheme 3).[a]

Entry	MOF	Substrate	Product	Product [%]
1	No catalyst		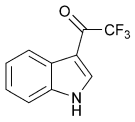	0
2	MIL-100(Sc)			8
3	MIL-100($Sc_{60}Fe_{40}$)			92
4	MIL-100($Sc_{60}Fe_{40}$)XS			87
5	MIL-100(Fe)			53
6	HKUST-1(Cu)			14
7	No catalyst		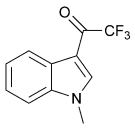	0
8	MIL-100(Sc)			7
9	MIL-100($Sc_{60}Fe_{40}$)			93
10	MIL-100($Sc_{60}Fe_{40}$)XS			85
11	MIL-100(Fe)			51
12	No catalyst		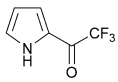	0
13	MIL-100(Sc)			9
14	MIL-100($Sc_{60}Fe_{40}$)			97
15	MIL-100($Sc_{60}Fe_{40}$)XS			92
16	MIL-100(Fe)			48
17	No catalyst	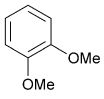	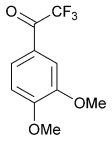	0
18	MIL-100(Sc)			3
19	MIL-100($Sc_{60}Fe_{40}$)			56
20	MIL-100($Sc_{60}Fe_{40}$)XS			51
21	MIL-100(Fe)			20
22	HKUST-1(Cu)			0

[a] Reactions carried out using 1 mmol of 2-methylindole and 1.2 mmol trifluoroacetaldehyde ethyl hemiacetal 4 mmol *tert*-butyl hydroperoxide 5 mL toluene/decene at room temperature for 6 h unless otherwise stated. Determined by $^{19}F\{^1H\}$ NMR using 1-fluoronaphthalene as internal standard; ^1H NMR also measured. Reactions 17–22 carried out at 90 °C over 16 h.

The progress of the reaction was followed by solution-state ^{1}H NMR spectroscopy and it was possible to see the evolution of the addition intermediate and the ketone product over time. The variation of the concentrations of reactant, intermediate, and product demonstrate the expected form for a sequential reaction (Figure 12).

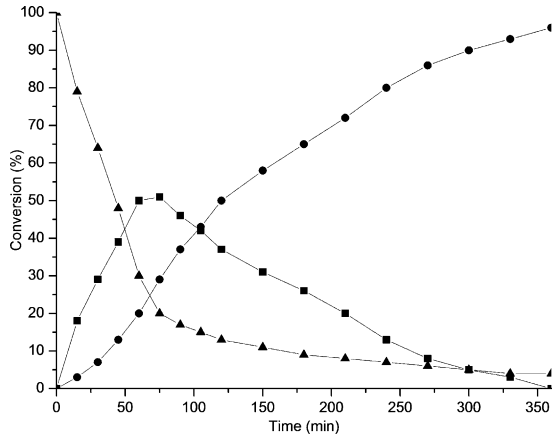

Figure 12. Conversion versus time for the tandem reaction of 2-methylindole with trifluoroacetaldehyde ethyl hemiacetal using MIL-100($Sc_{60}Fe_{40}$). Starting material (▲), Friedel–Crafts product (■), and oxidation product (●). ^{1}H NMR taken at regular intervals, 1-fluoronaphthalene used as internal standard.

The production of ketone is sigmoidal because the concentration of alcohol substrate increases to a maximum and then declines, so the rate of ketone formation reaches a maximum at around 50% conversion to the alcohol, and afterwards slows down as the concentration of the intermediate decreases.

Notably, although a simple physical mixture of MIL-100(Sc) and MIL-100(Fe) with the same Sc/Fe ratio also catalyzed the sequential reaction, lower conversions were achieved (78% cf. 95% after 31 h), suggesting that there is some advantage in combining both types of active sites within the same particle, possibly because the average diffusion path for the intermediate is reduced.

The results in Tables 6 and 7 show that MIL-100($Sc_{60}Fe_{40}$)XS was also very active in the tandem reaction, suggesting that both framework Fe^{3+} and nanoparticulate α-Fe_2O_3 are active in the oxidation step.

To ensure that the catalytic steps in the tandem reaction were fully heterogeneous, the Friedel–Crafts addition, the oxidation and the one-pot tandem reaction (Schemes 4, 5, and 3, respectively) were allowed to run for 2.5 h (for MIL-100($Sc_{60}Fe_{40}$) and MIL-100($Sc_{60}Fe_{40}$)XS) and then the catalyst removed by filtration. In each case the catalytic reaction stopped (Supporting Information). Furthermore, these solids can be re-used without loss of activity, and PXRD analysis of MIL-100($Sc_{60}Fe_{40}$) and MIL-100($Sc_{60}Fe_{40}$)XS after use as a catalyst in the tandem Friedel–Crafts addition and oxidation reaction of 2-methylindole with trifluoroacetaldehyde ethyl hemiacetal and *tert*-butyl hydroperoxide for 6 h indicates that the catalysts remain crystalline.

Finally, as we had shown it was also possible to introduce both Sc and Cr into trimer sites in MIL-100, and MIL-100(Cr) has recently been reported to be an active oxidation catalyst,[31] we investigated MIL-100($Sc_{60}Cr_{40}$) as a catalyst for the one-pot Friedel–Crafts addition and oxidation reaction of 2-methylindole with trifluoroacetaldehyde ethyl hemiacetal and tert-butyl hydroperoxide. Although 95% conversion of the reactant trifluoroacetaldehyde ethyl hemiacetal was observed, the catalyst was very unselective, so that along with 8% of the intermediate 2,2,2-trifluoro-1-(2-methyl-1H-indol-3-yl)ethanol and only 52% of the desired product 2,2,2-trifluoro-1-(2-methyl-1H-indol-3-yl)ethanone the ^{19}F NMR showed another seven peaks making up 35% of the fluorinated products. This illustrates the advantages of using the highly selective MIL-100(Sc,Fe) catalyst in this reaction.

These results establish that two catalytically active framework metals can contribute towards the development of new reaction sequences; the tandem deacetalisation–Friedel–Crafts addition–oxidation reaction reported herein has no precedent in homogeneous catalysis. Whilst other methods are available for the synthesis of trifluoroacylated aromatic compounds, such as Friedel–Crafts acylation using perfluoroacyl derivatives, the use of cheap and commercially available fluoral hemiacetal is attractive, and the only waste products are ethanol and *tert*-butanol, so products are readily obtained. The tandem catalytic activity demonstrated herein should be widely applicable. Remarkably, we have made use of aldehydes as intermediates under strongly oxidizing conditions with no sign of aldehyde oxidation products; presumably the Friedel–Crafts reaction takes place immediately as the hemiacetal is unmasked.

Conclusion

We report herein bifunctional catalysis over mixed-metal MOFs that are readily prepared and recyclable. These MIL-100(Sc,Fe) catalysts, in which Fe^{3+} cations as well as Sc^{3+} cations occupy framework sites that can become coordinatively unsaturated, can act as Lewis acid catalysts (via Sc^{3+} and Fe^{3+} sites) and oxidation catalysts (via the Fe^{3+} sites) both separately and together. The MIL-100 framework provides a robust, highly porous and three-dimensionally connected host for these active sites. The activity of the catalyst for both acid and oxidation catalysis under the same conditions (and in the presence of *tert*-butylhydroperoxide) has been demonstrated in a tandem process for making ketones from (hetero)aromatics and a hemiacetal. It should be possible to extend this approach of utilising more than one catalytically active metal in a MOF framework further by the incorporation of additional metal centres (molecular catalysts, or nanoparticles). This promises the introduction of some new catalytic chemistry, and more effective combined one-pot processes for the sustainable production of fine chemicals.

Experimental Section

For syntheses of mixed Sc,M-containing MIL-100 samples (M = Al, Cr, Fe), benzene-1,3,5-tricarboxylic acid (BTC, Aldrich, 95%), scandi-

um chloride solution (1.45 M) and a salt of the second metal (aluminium nitrate nonahydrate (99.9%, Sigma Aldrich), chromium chloride hexahydrate (96%, Sigma Aldrich) or iron (III) chloride hexahydrate (Aldrich)) were dissolved in the desired proportions in dimethylformamide (DMF; Acros, 98%, 10 mL). In each case the molar ratio of total trivalent metal cations to BTC was kept at 3:2 and molar ratios of Sc:M of 100:0, 80:20, 60:40, 60:40, and 80:20 were used, as well as others in some cases. The ratio of BTC to solvent DMF was kept at 2:600. In a typical preparation of a material of nominal MIL-100(Sc_{60},Fe_{40}) composition, benzene-1,3,5-tricarboxylic acid (BTC, Aldrich, 95%, 0.0908 g, 0.43 mmol), scandium chloride solution (1.45 M, 0.39 mmol, 0.27 mL), and iron (III) chloride hexahydrate (Aldrich, 0.26 mmol, 0.0701 g) were dissolved in dimethylformamide, DMF (Acros, 98%, 10 mL). The reaction mixtures were heated in a Teflon-lined steel autoclave at 383 K for 24 h. For the MIL-100(Sc,Fe)XS series, the molar ratio of total trivalent metal cations to BTC was kept at 3:2 and molar ratios of Sc:Fe of 2:2–5 were used. The ratio of BTC to solvent DMF was kept at 2:600.

The resulting solids were washed with ethanol and water and dried at 60 °C. Product identification was carried out using powder X-ray diffraction (PXRD). PXRD patterns were collected for MOFs using PANalytical Empyrean and STOE STADI P diffractometers using Cu $K_{\alpha 1}$ X-radiation ($\lambda = 1.54056$ Å). Adsorption isotherms for N_2 on the MIL-100 samples were obtained at 77 K using a Micromeritics Tristar II 3020. Prior to measurement of the isotherms, the samples were washed with methanol and activated under vacuum at 150 °C for 5 h. EDX measurements were obtained by a JEOL 5600 SEM with an Oxford INCA Energy 200 EDX system. Elemental analyses were performed on organic compounds and metal–organic frameworks by Elemental Analysis Service, London Metropolitan University, London, UK. ^{27}Al and ^{45}Sc NMR spectra were obtained using a Bruker Avance III 600 MHz spectrometer, equipped with a wide-bore 14.1 T superconducting magnet, at Larmor frequencies of 156.4 MHz for ^{27}Al and 145.8 MHz for ^{45}Sc. ^{13}C NMR spectra were obtained using a Bruker Avance III 400 MHz spectrometer, equipped with a wide-bore 9.4 T superconducting magnet, at Larmor frequencies of 400.16 MHz for ^{1}H and 100.6 MHz for ^{13}C. Powdered samples were packed into 4 or 2.5 mm ZrO_2 rotors and rotated at MAS rates between 12.5 and 30 kHz. Chemical shifts are given relative to TMS for ^{13}C, 1 M $Al(NO_3)_3$ (aq) for ^{27}Al and 0.2 M $ScCl_3$ (aq) for ^{45}Sc. For ^{13}C, spectra were acquired using cross-polarisation, with a contact pulse (ramped for ^{1}H) of 1.5 ms duration and ^{1}H decoupling (SPINAL64) was applied throughout acquisition. TEM images of MIL-100($Sc_{60}Fe_{40}$)XS were produced using a Jeol JEM 2011 HRTEM with an accelerating voltage of 200 kV. The samples were prepared by grinding the powder sample with acetone and depositing the solution on a Cu grid. HKUST-1(Cu) (Cu_3BTC_2) was prepared according to a published synthesis and characterised by PXRD (Supporting Information). Its BET surface area, determined by N_2 adsorption at 77 K, was 965 $m^2 g^{-1}$.

For all of the catalytic reactions, chemicals were purchased from commercial suppliers. Dry solvents were used in reactions that were carried out under N_2. Electrospray ionisation mass spectroscopy was performed with a Micromass LCT spectrometer, operated by Mrs Caroline Horsburgh at St Andrews University, or at the ESPSRC National Mass Spectrometry Service Centre, Swansea University, by using Waters ZQ4000, Thermofisher LTQ Orbitrap XL and Finnigan MAT 900 XLT Instruments. Thin layer chromatography was carried out on pre-coated 0.2 Å Machery-Nagel Polygram SIL G/UV254 silicon plates. Absorption under UV light was visualised as well as thermal decomposition after immersion in aqueous solution of potassium permanganate if required. Column chromatography was performed using Davisil silica gel Fluorochem 60 Å, particle size 35–70 μm. ^{1}H NMR, ^{13}C NMR, ^{19}F NMR, and ^{31}P NMR were carried out using a Bruker Avance 400 spectrometer at 400 Hz or Bruker Avance 300 spectrometer at 300 Hz. Chemical shift information for each signal is given in part per million (ppm) relative to trimethylsilane (TMS). Chemical shifts for ^{19}F are relative to $CFCl_3$ and ^{31}P relative to phosphoric acid. Methanol-washed, thermally activated MOF catalysts were used in a series of Lewis acid catalyzed Friedel–Crafts reactions of 2-methylindole and related compounds with trifluoroacetaldehyde ethyl hemiacetal to give alcohols. The oxidation of these alcohols was performed over MOFs using *tert*-butylhydroperoxide to give ketones, and for selected MOFs, the tandem, one-pot reaction was also performed. The amount of MOF catalyst used was 5 mol%, unless stated otherwise, calculated as the molar percentage of the available metal cation (Sc, Fe, Cr, Al, or Cu), of the reactant molecule. (For MIL-100 materials two out of three metal cations per trimer were considered available, with one in three coordinated by an anion). 100% conversion therefore relates to a turnover number of 20. Conversions were calculated for all reactions involving ethyl trifluoropyruvate or trifluoroacetaldehyde ethyl hemiacetal using ^{19}F{^{1}H} NMR using 1-fluoronaphthalene as an internal standard (^{1}H NMR was also measured for completeness), and in these reactions no peaks other than reactant, product, and internal standard were observed, except for the carbonyl ene reaction, when the hydrated reactant ethyl-3,3,3-trifluoro-2,2-dihydroxypropanoate was sometimes observed. For the conjugate addition of 2-methylindole to methyl vinyl ketone, conversions to product were measured by ^{1}H NMR. For some reactions the product was isolated and its identity and purity confirmed by NMR, MS, and elemental analysis. Detailed examples are given in the Supporting Information.

Acknowledgements

We thank Johnson Matthey and the EPSRC for an Industrial CASE award to L.M. We gratefully acknowledge the IAESTE UK for a scholarship to B.E. and we also thank the Leverhulme Trust (F/00 268/BJ), EPSRC (EP/J501542/1), and the EaStCHEM Research Computing Facility. We are grateful to Diamond Light Source for provision of beamtime for XAS and to Dr. Giannantonio Cibin for assistance in measuring the data on station B18. We gratefully acknowledge Dr. Alexandre Vimont at the Laboratoire Catalyse et Spectroschemie, ENSICAEN, Caen for help with measurement and analysis of the IR spectra. We thank all the technical staff at the University of St Andrews School of Chemistry for their assistance.

Keywords: bifunctional catalysts · heterogeneous catalysis · iron · scandium · tandem catalysis

[1] M. Eddaoudi, H. L. Li, T. Reineke, M. Fehr, D. Kelley, T. L. Groy, O. M. Yaghi, *Top. Catal.* **1999**, *9*, 105 – 111.
[2] J. L. C. Rowsell, O. M. Yaghi, *J. Am. Chem. Soc.* **2006**, *128*, 1304 – 1315.
[3] M. Latroche, S. Surblé, C. Serre, C. Mellot-Draznieks, P. L. Llewellyn, J.-H. Lee, J.-S. Chang, S. H. Jhung, G. Férey, *Angew. Chem. Int. Ed.* **2006**, *45*, 8227 – 8231; *Angew. Chem.* **2006**, *118*, 8407 – 8411.
[4] A. Corma, H. Garcia, F. X. L. Xamena, *Chem. Rev.* **2010**, *110*, 4606 – 4655.
[5] D. Farrusseng, S. Aguado, C. Pinel, *Angew. Chem. Int. Ed.* **2009**, *48*, 7502 – 7513; *Angew. Chem.* **2009**, *121*, 7638 – 7649.
[6] J. Lee, O. K. Farha, J. Roberts, K. A. Scheidt, S. T. Nguyen, J. T. Hupp, *Chem. Soc. Rev.* **2009**, *38*, 1450 – 1459.
[7] A. Dhakshinamoorthy, M. Alvaro, H. Garcia, *Catal. Sci. Technol.* **2011**, *1*, 856 – 867.

[8] A. Dhakshinamoorthy, H. Garcia, *Chem. Soc. Rev.* **2012**, *41*, 5262 – 5284.
[9] J. M. Thomas, *Proc. R. Soc. London Ser. A* **2012**, *468*, 1884 – 1903.
[10] J. M. Thomas, *Phys. Chem. Chem. Phys.* **2014**, *16*, 7647 – 7661.
[11] H. Furukawa, K. E. Cordova, M. O'Keeffe, O. M. Yaghi, *Science* **2013**, *341*, 974 – 985.
[12] B. Yuan, Y. Pan, Y. Li, B. Yin, H. Jiang, *Angew. Chem. Int. Ed.* **2010**, *49*, 4054 – 4058; *Angew. Chem.* **2010**, *122*, 4148 – 4152.
[13] F. G. Cirujano, F. X. Llabres i Xamena, A. Corma, *Dalton Trans.* **2012**, *41*, 4249 – 4254.
[14] A. Arnanz, M. Pintado-Sierra, A. Corma, M. Iglesias, F. Sanchez, *Adv. Synth. Catal.* **2012**, *354*, 1347 – 1355.
[15] F. G. Cirujano, A. Leyva-Perez, A. Corma, F. X. Llabres i Xamena, *ChemCatChem* **2013**, *5*, 538 – 549.
[16] F. Ke, J. Zhu, L.-G. Qiu, X. Jiang, *Chem. Commun.* **2013**, *49*, 1267 – 1269.
[17] D. T. Genna, A. G. Wong-Foy, A. J. Matzger, M. S. Sanford, *J. Am. Chem. Soc.* **2013**, *135*, 10586 – 10589.
[18] S. H. Cho, B. Q. Ma, S. T. Nguyen, J. T. Hupp, T. E. Albrecht-Schmitt, *Chem. Commun.* **2006**, 2563 – 2565.
[19] A. M. Shultz, O. K. Farha, D. Adhikari, A. A. Sarjeant, J. T. Hupp, S. T. Nguyen, *Inorg. Chem.* **2011**, *50*, 3174 – 3176.
[20] A. M. Shultz, A. A. Sarjeant, O. K. Farha, J. T. Hupp, S. T. Nguyen, *J. Am. Chem. Soc.* **2011**, *133*, 13252 – 13255.
[21] F. Song, C. Wang, J. M. Falkowski, L. Ma, W. Lin, *J. Am. Chem. Soc.* **2010**, *132*, 15390 – 15398.
[22] L. Ma, J. M. Falkowski, C. Abney, W. Lin, *Nat. Chem.* **2010**, *2*, 838 – 846.
[23] K. S. Jeong, Y. B. Go, S. M. Shin, S. J. Lee, J. Kim, O. M. Yaghi, N. Jeong, *Chem. Sci.* **2011**, *2*, 877 – 882.
[24] L. Alaerts, E. Seguin, H. Poelman, F. Thibault-Starzyk, P. A. Jacobs, D. E. De Vos, *Chem. Eur. J.* **2006**, *12*, 7353 – 7363.
[25] N. B. Pathan, A. M. Rahatgaonkar, M. S. Chorghade, *Catal. Commun.* **2011**, *12*, 1170 – 1174.
[26] K. Schlichte, T. Kratzke, S. Kaskel, *Microporous Mesoporous Mater.* **2004**, *73*, 81 – 88.
[27] A. Dhakshinamoorthy, M. Alvaro, H. Chevreau, P. Horcajada, T. Devic, C. Serre, H. Garcia, *Catal. Sci. Technol.* **2012**, *2*, 324 – 330.
[28] A. Dhakshinamoorthy, M. Alvaro, Y. K. Hwang, Y.-K. Seo, A. Corma, H. Garcia, *Dalton Trans.* **2011**, *40*, 10719 – 10724.
[29] N. V. Maksimchuk, O. V. Zalomaeva, I. Y. Skobelev, K. A. Kovalenko, V. P. Fedin, O. A. Kholdeeva, *Proc. R. Soc. London Ser. A* **2012**, *468*, 2017 – 2034.
[30] A. Dhakshinamoorthy, M. Alvaro, P. Horcajada, E. Gibson, M. Vishnuvarthan, A. Vimont, J.-M. Greneche, C. Serre, M. Daturi, H. Garcia, *ACS Catal.* **2012**, *2*, 2060 – 2065.
[31] O. A. Kholdeeva, I. Y. Skobelev, I. D. Ivanchikova, K. A. Kovalenko, V. P. Fedin, A. B. Sorokin, *Catal. Today* **2014**, *238*, 54 – 61.
[32] F. Vermoortele, B. Bueken, G. Le Bars, B. Van de Voorde, M. Vandichel, K. Houthoofd, A. Vimont, M. Daturi, M. Waroquier, V. Van Speybroek, C. Kirschhock, D. E. De Vos, *J. Am. Chem. Soc.* **2013**, *135*, 11465 – 11468.
[33] F. Vermoortele, M. Vandichel, B. van de Voorde, R. Ameloot, M. Waroquier, V. van Speybroek, D. E. de Vos, *Angew. Chem. Int. Ed.* **2012**, *51*, 4887 – 4890; *Angew. Chem.* **2012**, *124*, 4971 – 4974.
[34] J. P. S. Mowat, S. R. Miller, A. M. Z. Slawin, V. R. Seymour, S. E. Ashbrook, P. A. Wright, *Microporous Mesoporous Mater.* **2011**, *142*, 322 – 333.
[35] L. Mitchell, B. Gonzalez-Santiago, J. P. S. Mowat, M. E. Gunn, P. Williamson, N. Acerbi, M. L. Clarke, P. A. Wright, *Catal. Sci. Technol.* **2013**, *3*, 606 – 617.
[36] G. Férey, C. Serre, C. Mellot-Draznieks, F. Millange, S. Surblé, J. Dutour, I. Margiolaki, *Angew. Chem. Int. Ed.* **2004**, *43*, 6296 – 6301; *Angew. Chem.* **2004**, *116*, 6456 – 6461.
[37] A. Dhakshinamoorthy, M. Alvaro, H. Garcia, *J. Catal.* **2009**, *267*, 1 – 4.
[38] A. Dhakshinamoorthy, H. Garcia, *ChemSusChem* **2014**, *7*, 2392 – 2410..
[39] A. Le Bail, *Powder Diffr.* **2005**, *20*, 316 – 326.
[40] A. C. Larson, R. B. von Dreele, *General Structure Analysis System (GSAS)*, Los Alamos National Laboratory, Los Alamos, NM, **1994**.
[41] R. D. Shannon, *Acta Crystallogr. Sect. A* **1976**, *32*, 751 – 767.
[42] C. Volkringer, D. Popov, T. Loiseau, G. Ferey, M. Burghammer, C. Riekel, M. Haouas, F. Taulelle, *Chem. Mater.* **2009**, *21*, 5695 – 5697.
[43] C. J. Pickard, F. Mauri, *Phys. Rev. B* **2001**, *63*, 245101.
[44] M. D. Segall, P. J. D. Lindan, M. J. Probert, C. J. Pickard, P. J. Hasnip, S. J. Clark, M. C. Payne, *J. Phys. Condens. Matter* **2002**, *14*, 2717 – 2744.
[45] A. J. Dent, G. Cibin, S. Ramos, A. D. Smith, S. M. Scott, L. Varandas, M. R. Pearson, N. A. Krumpa, C. P. Jones, P. E. Robbins in *14th International Conference on X-Ray Absorption Fine Structure* (Eds.: A. DiCicco, A. Filipponi), IOP Publishing Ltd, Bristol, **2009**.
[46] B. Ravel, M. Newville, *J. Synchrotron Radiat.* **2005**, *12*, 537 – 541.
[47] H. Okudera, A. Yoshiasa, K. Murai, M. Okube, T. Takeda, S. Kikkawa, *J. Mineral. Petrol. Sci.* **2012**, *107*, 127 – 132.
[48] M. Newville, *J. Synchrotron Radiat.* **2001**, *8*, 322 – 324.
[49] T. B. Čelič, M. Rangus, K. Lázár, V. Kaučič, N. Z. Logar, *Angew. Chem. Int. Ed.* **2012**, *51*, 12490 – 12494.
[50] M. Faustini, J. Kim, G.-Y. Jeong, J. Y. Kim, H. R. Moon, W.-S. Ahn, D.-P. Kim, *J. Am. Chem. Soc.* **2013**, *135*, 14619 – 14626.
[51] A. Vimont, J.-M. Goupil, J.-C. Lavalley, M. Daturi, S. Surblé, C. Serre, F. Millange, G. Férey, N. Audebrand, *J. Am. Chem. Soc.* **2006**, *128*, 3218 – 3227.
[52] H. Leclerc, A. Vimont, J.-C. Lavalley, M. Daturi, A. D. Wiersum, P. L. Llewellyn, P. Horcajada, G. Férey, C. Serre, *Phys. Chem. Chem. Phys.* **2011**, *13*, 11748 – 11756.
[53] C. Volkringer, H. Leclerc, J.-C. Lavalley, T. Loiseau, G. Férey, M. Daturi, A. Vimont, *J. Phys. Chem. C* **2012**, *116*, 5710 – 5719.
[54] C. Otero Areán, C. Palomino Cabello, G. Turnes Palomino, *Chem. Phys. Lett.* **2012**, *521*, 104 – 106.
[55] M. L. Clarke, M. B. France, *Tetrahedron* **2008**, *64*, 9003 – 9031.
[56] A. Dhakshinamoorthy, H. Garcia, *Chem. Soc. Rev.* **2014**, *43*, 5750-5765..

Received: July 13, 2014
Revised: September 2, 2014
Published online on ■■ ■■, 0000

FULL PAPER

Metal–Organic Frameworks

L. Mitchell, P. Williamson, B. Ehrlichová, A. E. Anderson, V. R. Seymour, S. E. Ashbrook, N. Acerbi, L. M. Daniels, R. I. Walton, M. L. Clarke, P. A. Wright**

■■ – ■■

Mixed-Metal MIL-100(Sc,M) (M = Al, Cr, Fe) for Lewis Acid Catalysis and Tandem C–C Bond Formation and Alcohol Oxidation

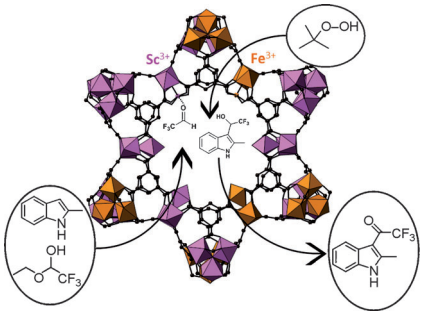

Two-in-one: The mixed-metal Sc^{3+} and Fe^{3+} form of the MOF MIL-100 was investigated. The metal cations are shown to be in trimeric $M_3O(O_2C–)_6$ units by MAS NMR and EXAFS spectroscopy. It is an excellent bifunctional catalyst for a tandem Friedel–Crafts addition/oxidation reaction that makes ketones from heteroaromatic compounds and a hemiacetal.